Acta Crystallographica Section D
Biological Crystallography
ISSN 0907-4449

Removing the invariant salt bridge of parvalbumin increases flexibility in the *AB*-loop structure

François Hoh,[a] Adrien Cavé,[a] Marie-Paule Strub,[b] Jean-Louis Banères[c] and André Padilla[a]*

[a]CNRS UMR 5048, INSERM U554, Université Montpellier 1 et 2, Centre de Biochimie Structurale, 29 Rue de Navacelles, 34090 Montpellier, France, [b]National Institutes of Health, Building 50, Room 3509, 50 Center Drive, Bethesda, MD 20892-8013, USA, and [c]CNRS UMR 5247, Université Montpellier 1 et 2, IBMM Faculté de Pharmacie, 15 Avenue Charles Flahault, BP 14491, 34093 Montpellier, France

Correspondence e-mail: andre.padilla@cbs.cnrs.fr

Received 20 January 2009
Accepted 27 March 2009

PDB Reference: R75A rat parvalbumin, 3f45, r3f45sf.

Parvalbumins (PVs) are calcium-buffer proteins that belong to the EF-hand family. Their N-terminal domain consists of two antiparallel helices *A* and *B* that make up a flat hydrophobic surface that is associated with the opposite side of the *CD* and *EF* binding sites. A single conserved Arg75–Glu81 salt bridge is buried in this hydrophobic interface. The structure of a rat PV mutant in which Arg75 was replaced by alanine was solved by molecular replacement. Unexpectedly, a large distance deviation of 7.8 Å was observed for the *AB* loop but not for the residues that flank the R75A mutation. The thermal stability of the calcium-loaded form is lower (T_m = 352.0 K; $\Delta T_m = -11.4$ K) than that of the wild-type protein and the apo mutant is unfolded at room temperature. Weaker calcium or magnesium affinities were also measured for the R75A mutant (Ca^{2+}: $K_1 = 4.21 \times 10^7\ M^{-1}$, $K_2 = 6.18 \times 10^6\ M^{-1}$; Mg^{2+}: $K_1 = 2.98 \times 10^4\ M^{-1}$, $K_2 = 3.09 \times 10^3\ M^{-1}$). Finally, comparison of the *B* factors showed an increase in the flexibility of the *AB* loop that is consistent with this region being more exposed to solvent in the mutant. The mutant structure therefore demonstrates the role of the salt bridge in attaching the nonbinding *AB* domain to the remaining protein core. Normal-mode analysis indeed indicated an altered orientation of the *AB* domain with regard to the *CD–EF* binding domains.

1. Introduction

Parvalbumins are members of the EF-hand family of calcium-binding proteins. They are highly stable soluble proteins of molecular weight 12 kDa that are easily isolated from a variety of vertebrate sources (Heizmann, 1984). The mammalian genome encodes one α isoform and one β isoform of parvalbumin (PV; Goodman & Pechere, 1977), with only one member of each being present in mammals. The widely distributed α-PV exhibits a very high affinity for calcium and is believed to serve as a calcium buffer. In contrast, oncomodulin (OM; Szatkowski *et al.*, 2001), the mammalian β-PV, displays a highly attenuated affinity for calcium that is consistent with a calcium-dependent regulatory function (Sakaguchi *et al.*, 1998). Exchange of bound Mg^{2+} for Ca^{2+} confers a major relaxation function to α-PV in excitatory cells, in muscles and in the brain (Kreiner & Lee, 2006). In muscles, by acting as a 'slow-onset' Ca^{2+} buffer, α-PV does not affect the rapid contraction phase but significantly increases the rate of relaxation, as demonstrated in $PV^{-/-}$ mice (Racay *et al.*, 2006). In the brain, PV is mostly known to be a marker of neuron populations (Wouterlood *et al.*, 2002; Reynolds *et al.*, 2004). Over-

expression of parvalbumin into normal adult myocardium increased cardiac relaxation *in vitro* (Wahr *et al.*, 1999) as well as *in vivo* (Szatkowski *et al.*, 2001) in normal hearts and improved diastolic dysfunction in two different rat models of senescence.

The structure of parvalbumin (Kretsinger & Nockolds, 1973) is constituted of the scaffold of the large family of EF-hand-containing proteins, which are characterized by helix–loop–helix (HLH; Kissinger *et al.*, 1999) ion-binding motifs (two helices pack together at an angle of ∼90°, separated by a loop region in which calcium binds). In the parvalbumin HLH structural motif, calcium is coordinated by one carbonyl O atom and the oxygen-containing side chains of five amino-acid residues or of four residues and a water molecule. The binding pocket itself is 12 residues in length, with alternate positions making an octahedral coordination shell around the ion. EF-hand motifs appear in pairs in calcium-binding protein structures; a small antiparallel β-sheet produces the pairing architecture.

The structures of many PVs from both lineages have been established by X-ray crystallography and various mutants have been prepared in order to define the role of the most conserved residues, particularly those involved in Ca^{2+} coordination. PV and galactose-binding protein (GBP; Drake & Falke, 1996; Drake *et al.*, 1997) have been used as model systems to study the roles of residues in EF-hands. It was shown that Gly substitutions of noncoordinating residues often yielded minor effects on metal binding, while substitutions of the coordinating or hydrophobic side chains at loop positions 1, 3, 5, 8 or 9 perturbed the stability or metal-binding parameters of GBP.

In rat PV, substitution of the first coordinating residue in the loop by Ala led to inactivation of the site (Cates *et al.*, 1999), while the substitution of the noncoordinating residue Phe102 by tryptophan affected neither the structure nor the affinity for ions, thus allowing the use of fluorescence techniques. The replacement of various coordinating and noncoordinating residues within the *CD* binding loop of rat OM led to the conclusion that only those involving positions 9 and 10 affected the affinity for calcium (Palmisano *et al.*, 1990).

Two distinct mechanisms have been proposed: the first, termed ground-state tuning, states that the presence of a long side chain at position 9 (such as Glu) adds stability to the metal–protein complex and the second, termed kinetic tuning, states that the height of the transition barrier of the binding reaction can be decreased by substituting Glu by neutral residues independently of the binding affinity (Drake & Falke, 1996). In the gateway model, the side chain at position 9 serves as a gate to control the rates of metal-ion binding and release. Kinetic control through in and out motions of the metal occur *via* the axial position guarded by the gateway residue (Drake & Falke, 1996) as observed in OM, in which an Asp-to-Glu

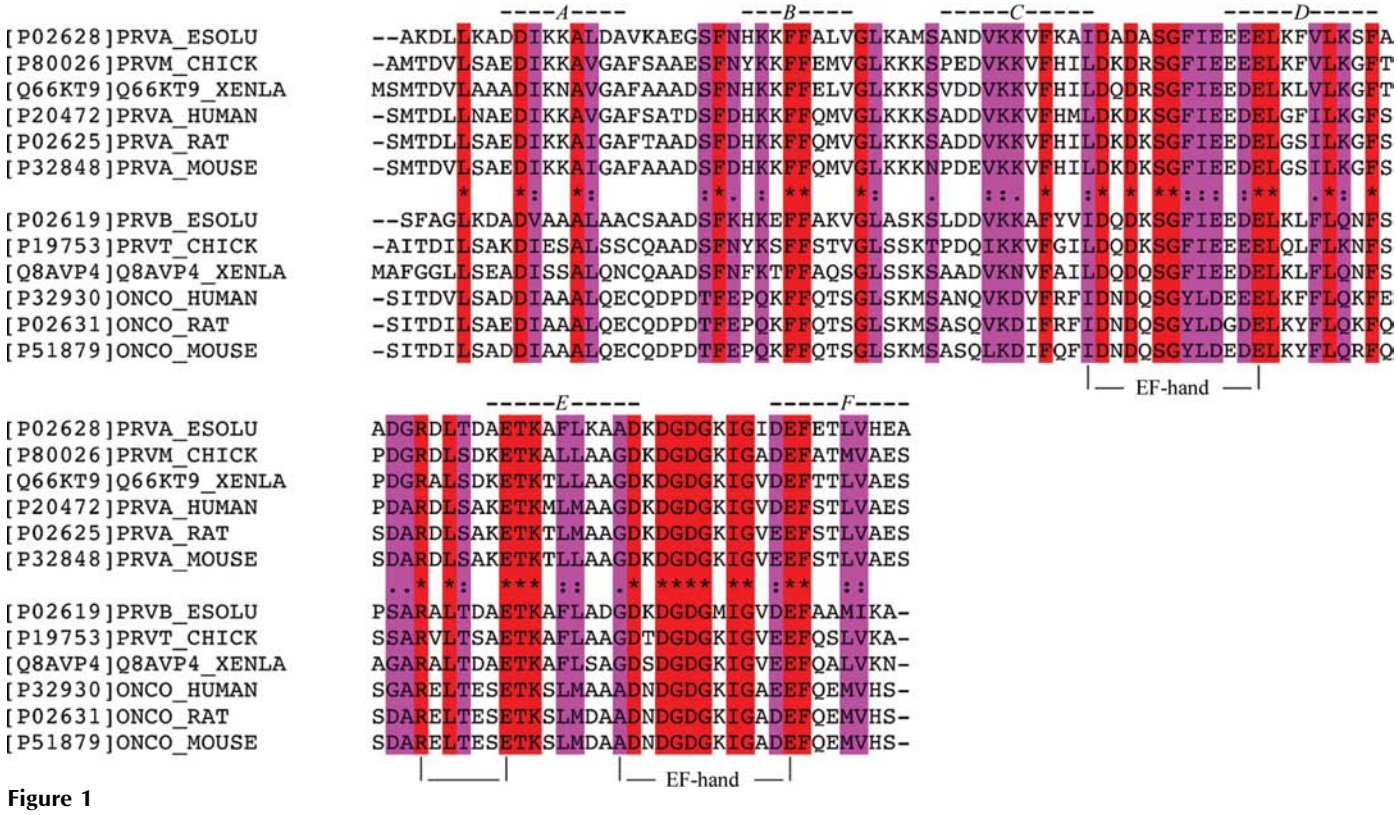

Figure 1
Sequences of fish (*Esox lucius*), chicken, *Xenopus laevis*, human, rat and mouse parvalbumins have been extracted from the SWISS-PROT data bank and aligned using the *ClustalW* server (http://www.ch.embnet.org/software/ClustalW.html). Strictly conserved residues are shown in red. A subset of these sequences is shown with secondary-structure assignments from the CaBp database (http://structbio.vanderbilt.edu/cabp_database/index.html). The limits of the helices are helix *A*, 8–17; helix *B*, 26–33; helix *C*, 40–50; helix *D*, 60–70; helix *E*, 79–89; helix *F*, 99–109. The calcium-binding sites *CD* and *EF* and the single Arg75–Glu81 salt bridge are indicated.

mutation at position 9 in the *CD* site increases the affinity for calcium (Golden *et al.*, 1989).

Interconversion of the *CD* and *EF* sites in OM can also be performed (Kauffman *et al.*, 1995), indicating that the context of the *CD* binding site exerts a major influence on the metal ion-binding properties of the site. Remote determinants have also been explored. The association of the *AB* and *CD–EF* domains from rat α-PV and β-PV have been studied by ultracentrifugation and ITC techniques and suggested that the *AB* domain modulates the calcium affinity of the *CD* and *EF* sites (Henzl, Agah *et al.*, 2004).

The *AB* site of PV is a nonfunctional vestigial EF-hand owing to the absence of oxygen-bearing residues in the central loop (Wnuk *et al.*, 1982). It is associated with the hydrophobic sides of the paired *CD* and *EF* sites (McPhalen *et al.*, 1991); its antiparallel helix–loop–helix arrangement makes a plate with one polar and one hydrophobic side that stacks on the hydrophobic basket formed by the *CD* and *EF* domains. The dynamics of ^{13}C (Alattia *et al.*, 1996) and ^{15}N (Baldellon *et al.*, 1998) NMR relaxation have demonstrated that the overall protein backbone is much more rigid compared with other EF-hand proteins. The *DE* linker (between the *CD* and *EF* sites) is not flexible when compared with other EF-hand-bearing proteins and its structure remained stable upon deletion of the *AB* domain (Thepaut *et al.*, 2001). Indeed, upon the removal of the *AB* domain from α-PV the calcium affinity of the remaining *CD–EF* fragment decreased by two orders of magnitude in the case of pike α-PV (Permyakov *et al.*, 1991) and by four orders of magnitude in the case of rat α-PV (Henzl, Agah *et al.*, 2003), suggesting that the evolution of the *AB* site to an abortive site was instrumental to the increase in the Ca^{2+} affinity of the *CD–EF* domain in PVs. Almost 30 different sequences of PV are found in lower and higher vertebrate sequence databases. A subset of these sequences is reported in Fig. 1. It is worth recalling that the level of sequence identity between these proteins is 50%, but the conserved residues are differently distributed among EF-hand pairs. Indeed, the *AB* site has the lowest level of identity (44%), followed by the *EF* (50%) and *CD* (53%) pairs. Additionally, the loop between helices *A* and *B* shows an even greater variance: only two residues out of eight are conserved in this loop, while four and eight residues out of nine are conserved in the *CD* and *EF* loops, respectively. The Arg75–Glu81 salt bridge, which is conserved in all PV sequences and structures, is found in the linker between the *CD* and *EF* domains (Fig. 1).

The aim of this work was to study this invariant salt bridge of the PV family at the structural level and to identify how it can modulate the Ca^{2+}/Mg^{2+} affinity. For this, we have produced, purified and crystallized a rat α-PV mutant in which the Arg75 residue has been substituted by an alanine. The X-ray structure indicates a major conformational rearrangement of the *AB* loop, whereas the *DE* linker still adopts the conformation observed in the wild-type or in the *AB* domain-deleted proteins. Together, the structural data presented here and comparisons with the wild-type structure suggest that the stabilization of the PV structure by the Arg75–Glu81 salt bridge mostly involves interactions with the nonbinding *AB* domain. We report interesting evidence for domain flexibility, which has been complemented by normal-mode calculations. These observations thus suggest a mechanism by which conformational changes are linked to salt-bridge structure stabilization.

Table 1
Summary of X-ray data collection.

Values in parentheses are for the highest resolution shell.

Space group	$P2_1$
Unit-cell parameters	
a (Å)	27.3
b (Å)	55.1
c (Å)	28.8
β (°)	105.5
Resolution range (Å)	27.7–2.0 (2.05–2.0)
No. of measured reflections	20256
No. of unique reflections	5480
Completeness (%)	97.5 (87.8)
$R_{\rm merge}$ (%)	4.7 (12)
$I/\sigma(I)$	16.7 (7.3)
Multiplicity	3.8 (3.1)
No. of working reflections	5229 (327)
No. of free reflections	251 (18)
$R_{\rm work}$	0.144 (0.200)
$R_{\rm free}$	0.205 (0.321)
R.m.s.d. bond lengths (Å)	0.016
R.m.s.d. bond angles (°)	1.60
No. of protein atoms	822
No. of Ca^{2+} atoms	2
No. of SO_4^{2-} molecules	2
No. of water molecules	155
Average B value for all atoms (Å^2)	12.08
Average B value for main chain (Å^2)	9.60
Average B value for side chain and waters (Å^2)	14.06
Average B value for Ca^{2+} atoms (Å^2)	7.39

2. Experimental procedures

2.1. Protein expression, mutagenesis and purification

The R75A mutation was introduced into the rat α-PV sequence using the QuikChange directed-mutagenesis kit (Stratagene) with the wild-type rat α-PV gene inserted in pGEMEX-1 as a template (Baldellon *et al.*, 1998). The mutation was confirmed by nucleotide sequencing. The plasmid containing the mutant PV sequence was used to transform *Escherichia coli* BL21 (DE3). The proteins were typically purified from 4 l cultures in LB broth containing ampicillin (100 µg ml^{-1}) as described previously (Thepaut *et al.*, 2001).

2.2. Crystallization, data collection and data processing

Crystals of R75A mutant rat α-PV (R75A PV) were grown using the hanging-drop vapour-diffusion method from a reservoir solution containing 3.2 *M* ammonium sulfate, 2% PEG 600, 100 m*M* MES pH 6. Protein solution at a concentration of 8.3 mg ml^{-1} was mixed with reservoir solution in a 2:1 ratio. Crystals grew at 290 K in about one week to dimensions of up to 0.05 × 0.05 × 1 mm. Prior to X-ray exposure, crystals were flash-frozen using the reservoir solution and 20% glycerol as a cryoprotectant and then placed on

the goniometer head. A data set from 28.2 to 2.0 Å resolution was collected at 100 K from a single crystal on a MAR Research image-plate detector using a Rigaku rotating-anode X-ray source operating at 40 kV and 90 mA with an X-ray wavelength of 1.54 Å. The $I/\sigma(I)$ value for the high-resolution data bin (Table 1) indicates that the resolution of the data was better than the resolution limit of 2.0 Å, which was imposed by the experimental setup. The program *MOSFLM* was used to index the frames, and *SORT* and *SCALA* (Collaborative Computational Project, Number 4, 1994) were used to scale the data. The crystals belonged to space group $P2_1$. Other details of the data and model are presented in Table 1.

2.3. Structure refinement

The coordinates of rat PV (PDB code 1rtp; McPhalen *et al.*, 1994) were used to generate a polyalanine chain. The initial model was calculated using the *EPMR* molecular-replacement program (Kissinger *et al.*, 1999) and refined with *REFMAC*5 (Collaborative Computational Project, Number 4, 1994). The first refinement run yielded an overall R of 33.0% for all data with $I > 2\sigma(I)$. A randomly selected 5% of the data were set aside for cross-validation (Brünger, 1993). Manual rebuilding of the model and addition of water molecules were performed using *Coot* (Emsley & Cowtan, 2004). An initial $2F_o - F_c$ map showed weak density for residues 18–24. Subsequent modifications included the adjustment of side chains and the addition of water molecules guided by $F_o - F_c$ maps alternating with refinement. Solvent molecules with B values greater than 50 Å^2 and density lower than 1.5σ were deleted. Refinement converged at R = 23.8% and R_{free} = 32.1%. The final model, containing 109 amino-acid residues, two SO_4^{2-} ions and 155 water molecules, yielded an R value of 14.4% and an R_{free} of 20.5%. The model was evaluated using *PROCHECK* (Laskowski *et al.*, 1993): all residues were in allowed regions of the Ramachandran plot.

2.4. Normal-mode analysis of R75A PV

ElNémo (Suhre & Sanejouand, 2004*a*,*b*), a web interface of the Elastic Network Model that provides a fast and efficient tool for the computation, visualization and analysis of low-frequency normal modes of macromolecules, was used to analyze each structure with the default parameter set. The input coordinate files for this analysis were those of R75A mutant calcium-loaded wild-type PV (Bottoms *et al.*, 2004; PDB code 1rwy) and apo PV (PDB code 2jww).

2.5. Differential scanning calorimetry (DSC) and isothermal titration calorimetry (ITC)

DSC data were collected using a MicroCal VP-DSC. All scans were obtained with a heating rate of 1 K min^{-1} after verifying that the width and shape of the transitions were independent of scan temperature at or below this value. The buffer (25 m*M* HEPES pH 7.5, 150 m*M* KCl) was filtered through a column equilibrated with Chelex-100 in order to remove divalent cations. Samples (2–4 mg ml^{-1}) were prepared using this buffer. Calcium was removed from the protein samples by 3% TCA precipitation and the samples were dialyzed to equilibrium against the buffer. Samples in presence of calcium were prepared with 25 m*M* HEPES pH 7.5, 150 m*M* KCl, 30 m*M* $CaCl_2$. The initial protein concentration was measured on a NanoDrop 1000 spectrophotometer. Reference buffer solutions and protein samples were degassed under vacuum for 5 min prior to loading. After obtaining a baseline scan with buffer alone in both sample and reference cells, the cells were refilled with the protein solution and buffer, respectively, and rescanned starting at 288 K. The data were analyzed with *DSC Origin* 7.0 software, fitting ΔH_d, ΔC_p and T_m. ΔC_p was also estimated from the difference between the extrapolated pre-transition and post-transition baselines at the melting temperature. The apo R75A PV samples were also rescanned starting at 278 K.

ITC was performed in a MicroCal VP-ITC calorimeter at 298 and 278 K. Apoprotein samples were prepared as indicated above. Following thermal equilibration, titrant additions were made at 240 s intervals to the 1.41 ml protein samples by adding 5 µl aliquots of 1 m*M* Ca^{2+} to protein samples (87 and 56 µ*M*) in 25 m*M* HEPES pH 7.5, 150 m*M* KCl. The protein concentration was also measured at the end of the experiment by recording UV spectra and corrected for dilution. Magnesium titrations were performed at 278 K by adding 5 µl aliquots of 4 m*M* Mg^{2+} to a protein sample at 198 µ*M* in the same buffer. Heat effects were integrated with *ITC Origin* 7.0 software.

3. Results

3.1. Structure of R75A PV

Structural investigation using homonuclear two-dimensional NMR experiments was initially performed with the calcium-loaded R75A PV and showed a good dispersion of chemical shifts consistent with the protein being folded and homologous to the wild-type protein. Sequence assignments were performed using COSY, TOCSY and NOESY spectra according to a standard strategy (Wüthrich, 1986). However, several resonances belonging to residues in the *AB* loop were missing for the mutant at room temperature, indicating fast exchange with the solvent and/or conformational flexibility of these residues. The low number of NMR-derived constraints for residues in this region of the protein resulted in a poorly defined *AB*-loop structure. In parallel, crystallization trials successfully gave well diffracting crystals. The structure solved by MR (see §2) is well defined with good statistics (Table 1). The Matthews coefficient of 1.78 Å^3 Da^{-1} corresponds to a low solvent content of the crystal of only 31%. The Ramachandran plot shows 97% of the residues in most favoured regions and 3% in additional allowed regions. Calcium ions are bound to the *CD* and *EF* sites. Ion coordination in the *EF* site also involves a water molecule. Overall, the structures of wild-type and R75A mutant α-PV superimpose well, with a r.m.s.d. of 1.32 Å on C^α atoms (Fig. 2). The calcium-binding EF-hands, the junction segment between the *D* and *E* helices and the *AB* helices have very similar structures in the wild-

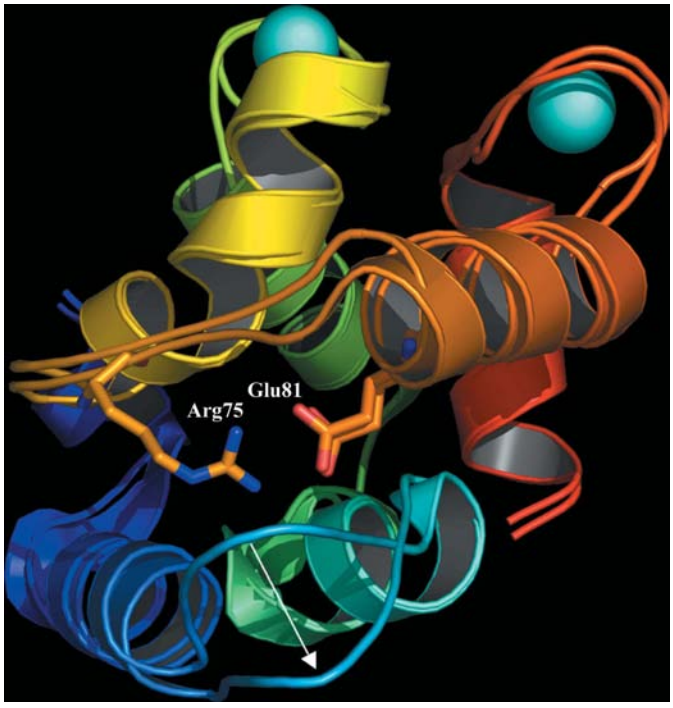

Figure 2
Superimposition of wild-type rat α-PV and R75A PV structures. The colour-coding of the helices is the same in both structures, from helix *A* in dark blue to helix *F* in red. The Arg75–Glu81 salt bridge in the wild-type structure is shown. Residue Glu81 from R75A PV is also displayed. The arrow indicates the main structural deviation at residue Ala21 between the wild type and the mutant structure. Calcium ions are shown in cyan.

type protein and in R75A PV. In all PV structures determined to date the Arg75–Glu81 salt bridge displays the same geometry (Fig. 3*a*). It makes an extensive network of hydrogen bonds with two sets of neighbouring residues in the *DE* linker (residue 78) and in the *AB* loop. Distances corresponding to hydrogen bonds between Glu81 and residues 22, 23 and 24 in the *AB* loop are shown in Fig. 3(*a*). There is also a short distance between Arg75 N^{ε} and the CO of residue 18.

In the R75A PV structure, the *AB* loop is displaced from the *DE*-linker region. The arrow in Fig. 2 indicates the main deviation of the backbone in the *AB* loop, which rises to 7.8 Å for the C^{α} atom of Ala21. We notice that the large distances between Glu81 and the *AB* loop in the R75A mutant are not compatible with hydrogen bonds. Careful analysis of the structure shows extensive molecular packing in this region, with one hydrogen bond between Phe18 CO and Ala40 N of a symmetry-related molecule. All other intermolecular contacts with the *AB* loop involve four symmetry-related water molecules, indicating high solvent accessibility.

The *B* factors shown in Fig. 4 display a similar profile along the sequence. However, an increase in *B* factors is observed for the *AB*-loop residues in the R75A mutant, indicating higher flexibility in this region. This is in agreement with our NMR data, in which weak cross-peak intensities were observed for *AB*-loop residues. Lower *B*-factor values are observed in the *EF* site in the R75A mutant, suggesting a coupling of the *AB* and *CD–EF* domain dynamics. This behaviour suggests that in wild-type PV the dynamics of the

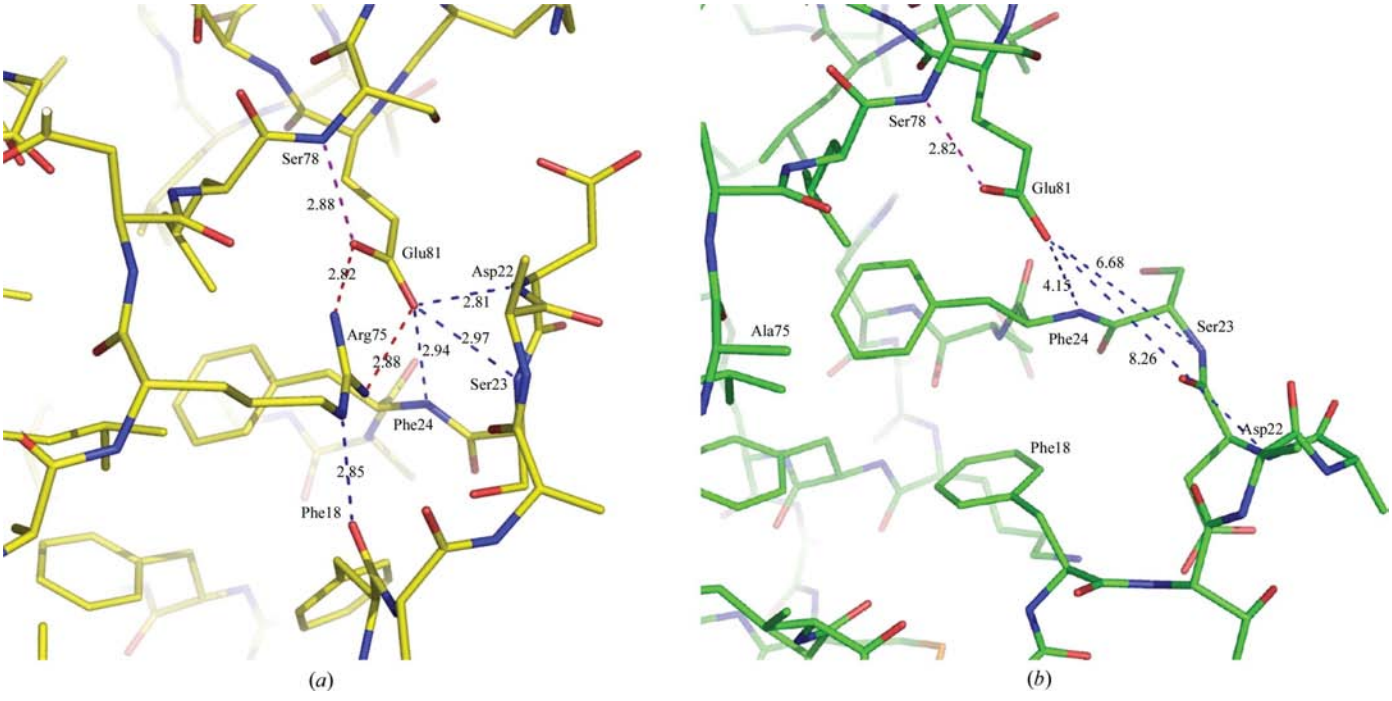

Figure 3
(*a*) View of the Arg75–Glu81 salt bridge of rat α-PV. Hydrogen-bond distances are shown in red for the salt bridge and in blue for hydrogen bonds involving residues 18–24 of the *AB* loop. (*b*) View of the R75A mutant with the distances indicated. The views are slightly different in order to clearly show the distances.

Table 2
Summary of DSC data on wild-type (wt) and mutant rat parvalbumins.

n.d., not determined.

Protein	T_m (K)	ΔT_m (K)	ΔH_d (kJ mol^{-1})	$\Delta\Delta G_{conf}$† (kJ mol^{-1})	$\Delta\Delta H_{conf}$‡ (kJ mol^{-1})	$-T\Delta\Delta S_{conf}$ (kJ mol^{-1})
Wt α-PV	363.4 ± 0.4		353 ± 3			
R75A PV	352.0 ± 0.2	−11.4	279 ± 3	−11.3	43.1	−54.4
Apo wt α-PV	308.1 ± 0.2		157 ± 15			
Apo R75A PV	282.6§	−25.5	n.d.	−13.0	54.4	−67.4

† $\Delta\Delta G_{conf} = \Delta T_m \Delta H_{dwt}/T_{mwt}$. ‡ $\Delta\Delta H_{conf} = -\Delta T_m \Delta C_{pwt}$. § Estimated value.

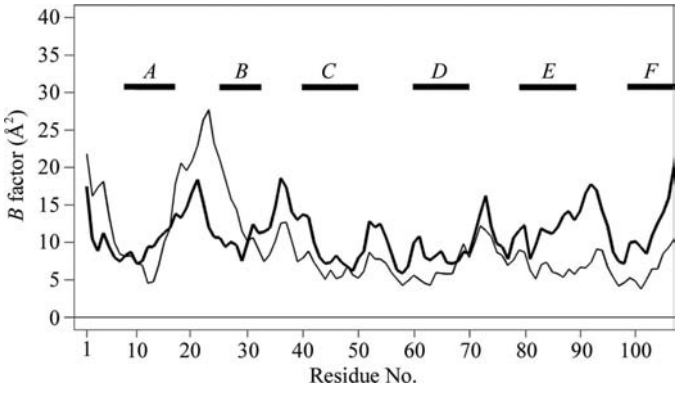

Figure 4
B-factor plot of backbone atoms for wild-type PV (dark lines) and R75A PV. Values for wild-type PV are averaged values over the three molecules in the asymmetric unit (PDB code 1rtp).

AB domain are reduced at the expense of increased motion in the rest of the molecule.

Together, the data are consistent with the *AB* loop in R75A PV being more exposed to the solvent and more flexible than that in the wild-type structure. Remarkably, residues close to Arg75 in the sequence remain at similar positions in the wild-type and mutant structures. Glu81 superimposes well and residues 75–81 do not display increased flexibility. This comparison indicates that the absence of the Arg75 guanidinium group interacting with the Glu81 carboxylate results in the loss of four hydrogen bonds. We conclude that removing the salt bridge does not alter the overall PV structure but adds flexibility and solvent accessibility to the *AB* loop.

3.2. Comparison of rat α-PV and R75A PV thermal stability

Scanning calorimetry data for wild-type rat α-PV and R75A PV obtained in 0.150 *M* KCl pH 7.5, 30 m*M* $CaCl_2$ were analyzed and the consequent thermodynamic parameters are reported in Table 2. Under these conditions, the wild-type protein denatures at 363.4 K, with an accompanying enthalpy change of 353 ± 3 kJ mol^{-1}. Under the same conditions, the R75A mutant denatures at 352.0 K, with an enthalpy change of 279 ± 3 kJ mol^{-1}. The mutation R75A therefore significantly lowers the conformational stability, lowering the T_m value by 11.4 K. Assuming that ΔC_p (ΔC_{pwt} = 3.87 ± 0.25 kJ mol^{-1} K^{-1} and ΔC_{pR75A} = 3.688 ± 0.21 kJ mol^{-1} K^{-1}) is unaltered by the mutation (ΔC_p is determined by the increase in the solvent-accessible apolar surface upon protein unfolding, which is expected to be similar for both proteins; Henzl & Graham, 1999) implies that the conformational free energy, $\Delta\Delta G_{conf}$, has been reduced by about 11.3 kJ mol^{-1} for the Ca^{2+}-bound mutant. Under the same conditions, the wild-type apoprotein denatures at 312.1 K, with an enthalpy change of 156 ± 15 kJ mol^{-1}. Similar values have previously been reported (Henzl *et al.*, 2000) in 100 m*M* KCl, 10 m*M* EDTA pH 7.4 buffer (T_m = 308.4 K and ΔH_d = 153 kJ mol^{-1}). Since it was not possible to acquire and analyze similar data for the apo R75A mutant because the protein was already unfolded at room temperature, we decided to record the experiment starting at the lower temperature of 278 K. A complete DSC transition could still not be recorded, but we observed a truncated peak from which a T_m value of 282.6 K (ΔT_m = 25.5 K) can be approximated for the apo R75A mutant. This again indicates a conformational free-energy ($\Delta\Delta G_{conf}$) reduction of about 13 kJ mol^{-1} for the apo mutant. No baseline subtraction was attempted and so ΔC_p could not be obtained in this case.

3.3. Comparison of rat α-PVand R75A PV ITC data

Apo R75A PV was initially titrated with $CaCl_2$ at 298 K. Because the protein is denatured at 298 K, the apparent enthalpy of Ca^{2+} binding at this temperature is large (see Table 3) and includes contributions from folding and from binding. For this reason, the analysis of Ca^{2+} and Mg^{2+} binding was conducted at 278 K (Figs. 5*a* and 5*b*). At this temperature, we expect that most of the protein is essentially in the native state and the data are fitted well by a non-equivalent two-site binding model. At 278 K, as the PV binding sites become saturated with calcium (Fig. 5*a*), the net change in heat associated with an injection event is greatly reduced. Estimates of the K_1 and K_2 association constants derived from calorimetric experiments are shown in Table 3 in comparison with similar data that have been published previously. As observed for the R75A mutant, the mutation decreases the Ca^{2+} affinity by about two orders of magnitude when compared with the wild-type protein. The first binding constant is reduced by 70-fold and the second by 107-fold, indicating that in the mutant both binding events become less effective than in the wild-type protein. The R75A α-PV mutant has Ca^{2+}-binding constants that are very similar to those for rat β-PV, which are reported for comparison in Table 3. Similarly, the mutation decreases the Mg^{2+} affinity by only one order of magnitude (a sevenfold and twelvefold decrease for the first and second binding event, respectively). The magnesium affinities are generally about four orders of magnitude lower than the calcium affinities (Henzl, Larson *et al.*, 2003).

Table 3
α-PV and R75A PV divalent ion-binding properties.

n.d., not determined.

Protein	Reference†	Ca^{2+} values				Mg^{2+} values			
		K_1 (M^{-1})	H_1 (kJ mol^{-1})	K_2 (M^{-1})	H_2 (kJ mol^{-1})	K_{1M} (M^{-1})	H_{1M} (kJ mol^{-1})	K_{2M} (M^{-1})	H_{2M} (kJ mol^{-1})
α-PV (278 K)	*a*	2.94×10^9	−15.2	6.59×10^8	−17.7	2.17×10^5	18.5	3.71×10^4	9.59
R75A PV (278 K)	*b*	$4.21 \times 10^7 \pm 0.8 \times 10^7$	−8.37 ± 0.21	$6.18 \times 10^6 \pm 0.9 \times 10^6$	−6.36 ± 0.4	$2.98 \times 10^4 \pm 4.9 \times 10^3$	8.20 ± 0.17	$3.09 \times 10^3 \pm 2.5 \times 10^2$	26.6 ± 0.4
R75A PV (298 K)	*b*	$1.49 \times 10^7 \pm 0.3 \times 10^7$	−99.6 ± 14.7	$7.74 \times 10^6 \pm 1 \times 10^6$	−41.0 ± 10.4	n.d.	n.d.	n.d.	n.d.
β-PV (298 K)	*a*	3.45×10^7	−23.0	3.36×10^6	−14.4	1.40×10^4	8.46	2.80×10^2	21.6

† (*a*) Henzl, Larson *et al.* (2003, 2004); (*b*) this work.

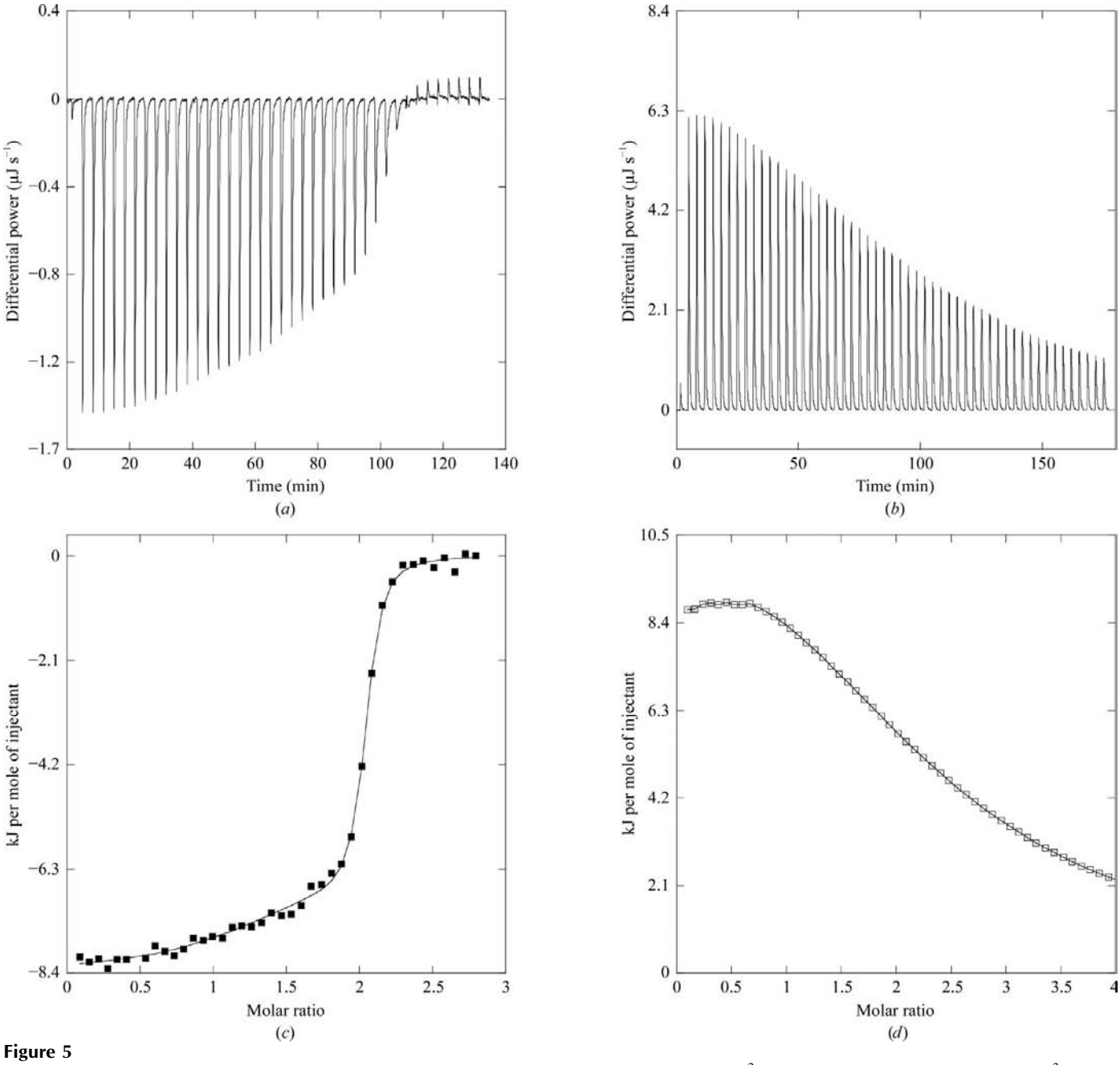

Figure 5
(*a*, *b*) Divalent ion-binding behaviour of rat R75A PV: representative raw ITC data. (*a*) 1.0 m*M* Ca^{2+} *versus* 56 µ*M* R75A PV; (*b*) 4 m*M* Mg^{2+} *versus* 198 µ*M* R75A PV. (*c*) Global least-squares analysis of ITC data for Ca^{2+} and (*d*) Mg^{2+} titration.

4. Discussion

Salt bridges in proteins play important roles in many functions (Zhou & Xu, 2003; Grove, 2003; Dong *et al.*, 2003; Yano & Poulos, 2003) and in intersubunit interactions within protein complexes (Marti & Bosshard, 2003; Kretsinger & Schneider, 2003). A salt bridge with favourable geometrical positioning of the interacting side-chain charged groups, as is the case for the Arg75–Glu81 salt bridge in PV, is likely to be stabilizing anywhere in the protein structure (Kumar & Nussinov, 1999). Salt bridges that exist in complex networks of many salt bridges have a greater tendency to stabilize a protein (Marqusee & Sauer, 1994) and most networked salt bridges occur in secondary-structure domains other than an α-helix or a β-sheet. About 64% of all salt bridges occur in α-helices (Sarakatsannis & Duan, 2005). Analyzing the residue separation of salt bridges indicated a sharp drop in frequency beginning at a residue separation of five, suggesting that most salt bridges occur in α-helical secondary structures. The structural and functional roles of the conserved Arg5–Glu13 salt bridge have been investigated in α-defensins (Wu *et al.*, 2005) and the salt bridge was reported to be necessary for the stability of defensin *in vivo*. In PV, the Arg75–Glu81 salt bridge has a residue separation of seven and does not occur in a helical structure. It is supposed to contribute to the overall protein stability, as indicated by a previous study involving chemical modification of Arg75 (Gosselin-Rey *et al.*, 1973). These authors found that modifying the single arginine in pike parvalbumin with 1,2-cyclohexanedione led to a reduced percentage of α-helicity as demonstrated by circular dichroism, a reduction in the Ca^{2+} content associated with the protein by 50–25% in the modified protein compared with the native protein and the loss of two antigenic determinants. They concluded that the arginine residue plays a key role in the tertiary structure of the molecule.

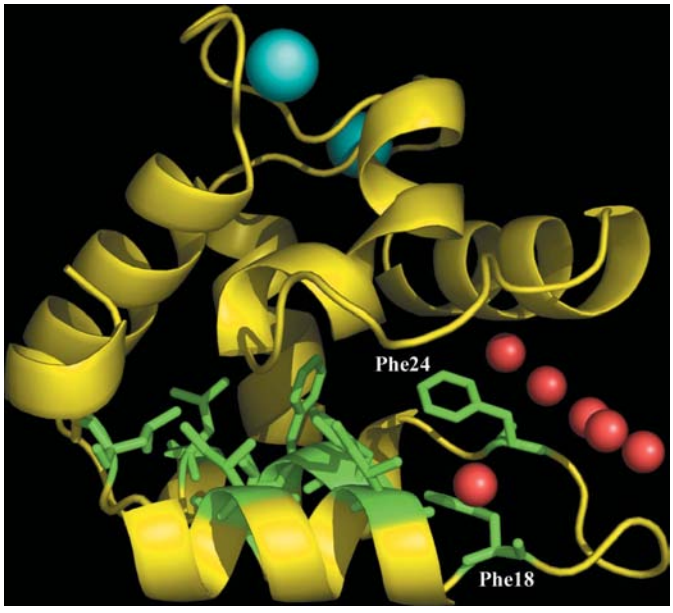

Figure 6
View of the hydrophobic interface between the *AB* and *CD–EF* domains in the R75A PV structure. Calcium ions are in cyan. Side chains of hydrophobic residues in *AB* are shown as sticks in green. The spheres in magenta show water molecules inserted between *AB* and *CD–EF*.

Here, we determined the structure of a mutant of rat α-PV without the salt bridge. Based on its X-ray structure, the mutant still displays the same fold as that of wild-type PV. The secondary-structure elements are clearly similar in both structures and we did not observe a loss of helical content. While thermal stability is reduced for the Ca^{2+}-loaded mutant, its T_m value still remains rather high (T_m = 352.0 K). Thus, removing the salt bridge has no dramatic effect on the calcium-bound protein structure, as previously postulated (Gosselin-Rey *et al.*, 1973). It is probable that the conjugation of 1,2-cyclohexanedione with Arg75 had other effects.

The data presented here for the R75A mutant indicate that the structure of the *CD–EF* binding domains is not perturbed by this single mutation. From comparison of the calcium-loaded wild-type and mutant proteins, we show that the structural differences are local, involving the loss of four hydrogen bonds in the mutant structure. Thermal stability is reduced for the Ca^{2+}-loaded R75A mutant, resulting in a loss of 11.3 kJ mol^{-1} of conformational free energy compared with the wild-type protein. The stability loss is even greater in the case of the apoprotein, with a $\Delta\Delta G_{conf}$ of -13.0 kJ mol^{-1}. The ion-free R75A PV mutant was already unfolded at room temperature (approximate T_m of 282.6 K).

The first binding event at 298 K is strongly exothermic (-99.6 kJ mol^{-1}) because it is linked to folding. The affinity is reduced because a substantial fraction of the intrinsic binding free energy is used to promote structural rearrangement from the apo to the Ca^{2+}-bound conformation. Despite 49% sequence identity (Gillen *et al.*, 1987), rat α-PV and β-PV exhibit distinct divalent ion-binding affinities (Hapak *et al.*, 1989; Cox *et al.*, 1990). The ΔG° for Ca^{2+} binding is about 16–20 kJ mol^{-1} more favorable for the α isoform. Because energy need not be expended to isomerize the protein, the net free-energy change that accompanies divalent ion binding for the later protein is more favourable. The structural data presented for the Ca^{2+}-free rat α isoform, for which the apo and Ca^{2+}-loaded proteins exhibit very similar tertiary structures (Henzl & Tanner, 2008), are compatible with this argument. Indeed, for the R75A PV mutant at 278 K the Ca^{2+} and Mg^{2+} affinity was still lower than that of the wild-type protein, which is consistent with its lower stability. Accordingly, the binding enthalpies for Ca^{2+} binding are 7–11 kJ mol^{-1} more favourable in the case of wild-type PV.

Several empirical methods have been developed to relate ΔC_p to changes in solvent-accessible area. According to the Freire–Murphy formalism (Xie & Freire, 1994; Murphy & Freire, 1992), the changes ΔASA_{ap} and ΔASA_{pol} in accessible polar and apolar surface areas, respectively, are related to ΔC_p and $\Delta H(333)$, which is the measured or extrapolated enthalpy change (Xie & Freire, 1994) at 333 K. We calculated the ΔASA_{ap} and ΔASA_{pol} of proteins with the thermodynamic parameters listed in Tables 2 and 3. The denaturation of calcium-loaded wild-type PV is accompanied by the exposure of 3026 and 3315 Å^2 of polar and apolar surface area, respectively. The denaturation of calcium-loaded R75A PV is

accompanied by the exposure of 2510 and 3405 Å^2 of polar and apolar surface area, respectively. The ΔASA_{pol} and ΔASA_{ap} values were also calculated on the basis of the structures using the *NACCESS* (Hubbard & Thornton, 1993) program with a probe radius of 1.4 Å and a slice width of 0.25 Å, as described in Xie & Freire (1994). The calculated ΔASA_{pol} and ΔASA_{ap} values of 2403 and 3417 Å^2, respectively, for R75A PV are in agreement with the experimental values. Using the NMR apo α-PV (PDB code 2jww) and calcium-loaded α-PV (PDB code 1rtp) structures, we obtained similar values of ΔASA_{ap} (3335 and 3411 Å^2, respectively) and ΔASA_{pol} (2262 and 2386 Å^2, respectively). Using the parameters listed in Tables 2 and 3, we found greater polar and apolar surface changes for the calcium-loaded α-PV, but these were within the error limits (Xie & Freire, 1994) of $\pm$ 9% for the calculated ΔC_p value. However, for apo α-PV the thermodynamic parameters gave an apolar surface change ΔASA_{ap} of 2450 Å^2, which is smaller than the value estimated from the NMR structure (ΔASA_{ap} = 3335 Å^2), indicating that the structure of the apo protein in K^+ solution is slightly less compact than the structure determined by NMR in Na^+ solution. The binding of Na^+, but not of K^+, has a major stabilizing effect on rat α-PV (Henzl *et al.*, 2000).

The X-ray structure of R75A PV also shows that the *AB* loop has increased flexibility when the salt bridge is removed. The interface between the *AB* and *CD–EF* domains is illustrated in Fig. 6. It is relatively flat and has hydrophobic character. The two hydrophobic residues Phe18 and Phe24 constitute the two limits of the *AB* loop and both are members of the hydrophobic interface. The removal of Arg75 (by mutation) affects the backbone structure of these two residues by removing backbone hydrogen bonds between Phe18 and Arg75 and between Phe24 and Glu81. This destabilization propagates, distal from the *A* and *B* helices, within the *AB* loop, leading to increased flexibility. As shown in Fig. 6, water molecules are now inserted into this opened region of the protein at a similar location to where the *AB* loop lies in the wild-type structure. Previous studies using ^{15}N NMR relaxation indicated that the *AB* domain of rat α-PV displayed a continuous increase in flexibility compared with the more rigid *CD–EF* binding domains (Baldellon *et al.*, 1998), with the *AB* loop itself having the highest degree of mobility. Faster NH-exchange rates for residues in *AB* than those in *CD–EF* were also measured for NH exchange using NMR techniques (Baldellon *et al.*, 1992). Opening of the *AB* domain was proposed as a mechanism to explain such fast exchange rates. We may also assume local unfolding and thus weakening of hydrophobic forces within the interface, permitting penetration of water molecules takes place.

Exploration of the molecular motion of biological molecules and their assemblies by simulation approaches such as molecular dynamics has provided a significant insight into structure–function relationships for small biological systems. Normal-mode analysis provides an alternative to molecular dynamics for the study of the motion of macromolecules. The timescale accessible to theoretical work is extended with normal-mode analysis and this approach has been proven to be extremely useful for studying the collective motion of biological systems (Go *et al.*, 1983; Levitt *et al.*, 1985). It has recently been shown that half of known protein movements can be modelled using two low-frequency normal modes. The applications of NMA cover wide areas of structural biology such as the study of protein conformational changes upon ligand binding, membrane-channel opening and closure, potential movements in the ribosome and viral capsid maturation. The low normal modes generally describe the most collective movements of a protein. In our case, the largest contribution arises from modes 8 and 9, which contribute to 45% of the motions. Note that the first mode (mode 7) in NMA is a 'trivial' very localized (*AB* loop) mode, so that mode 8 is the first nontrivial lowest frequency mode. When we examined the nature of the deformations along these two modes (modes 8 and 9), we observed that the *AB* domain rotates along the *C* helix. This movement moves helices *A* and *B* away from their initial positions (Fig. 7). The binding-site domain (*CD–EF*) superimposes well among all the frames, with the *BC* loop having the greatest screw displacement. Unexpectedly, the *AB* motion does not correspond to opening, but the entire *AB* domain slips on the *CD–EF* interface. We also calculated ΔASA_{pol} and ΔASA_{ap} from the various structures of mode 8 and found them to be close to the initial structure, with the maximum deviations with the last structure among the frames of 2730 and 3990 Å^2, respectively. These values indicate compaction of the structure along mode 8. Similar NMA calculations have been performed with the wild-type α-PV (PDB code 1rwy) and wild-type apo α-PV (PDB code 2jww) structures. They did not reveal similar domain movements. We also tried TLS refinements of the R75A PV data. However, these procedures did not improve the *R* factor, probably

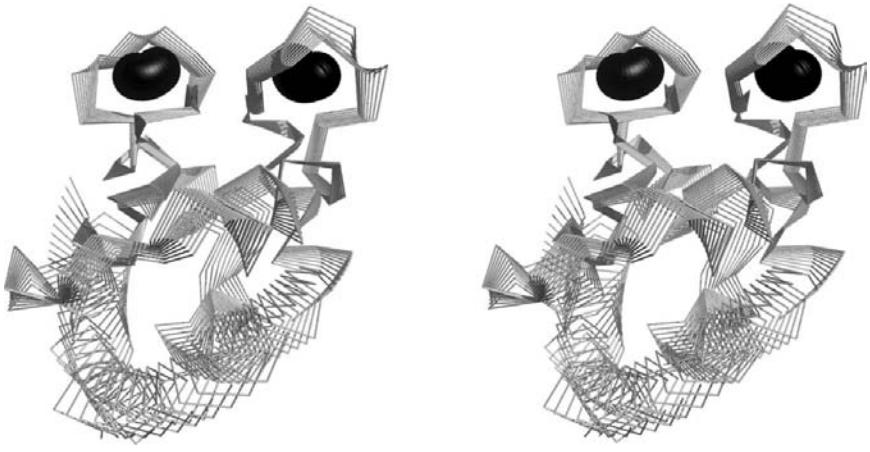

Figure 7
Stereoview of the superposed R75A PV of normal mode 8. The C^α trace of the superposed coordinates showing the movement of the *AB* domain. Calcium ions are shown in black.

owing to the packing of the crystal structure and an already low *R* factor (Table 1).

The main force favouring protein compaction in aqueous solvent is the hydrophobic effect. Interestingly, independent *AB* domains can associate with *CD–EF* entities (Henzl, Agah *et al.*, 2004) through their respective hydrophobic surfaces. Studies of chimeric PV in which *AB* domains from α-PV or β-PV were interconverted with *CD–EF* domains of β-PV or α-PV, respectively, have shown that the Ca^{2+} affinity is modulated by interactions between the *AB* and *CD–EF* domains (Henzl, Agah *et al.*, 2004). The data presented suggested that the β-PV *AB* fragment associates less avidly with *CD–EF* fragments and also that the β-PV *AB* fragment was less effective than the α-PV *AB* fragment at promoting Ca^{2+} chelation by the *CD–EF* fragment. Whereas α-PV *AB* is more susceptible to proteolysis than β-PV *AB*, it was suggested that the latter possesses a defined tertiary structure which renders a significant energetic cost, explaining the smaller gain in Ca^{2+} affinity. It is intriguing that residue 18 in α-PV is occupied by a bulky hydrophobic residue, whereas it is a small hydrophobic cysteine residue in β-PV (Nakayama *et al.*, 1992). This sequence difference may also account for the differential behaviour between the α-PV and β-PV *AB* fragments. Interestingly, study of the impact of proline residues substituting at sequence positions 21 and 26 (*AB* loop) on parvalbumin stability and ion-binding properties has shown that they do not necessarily influence the divalent-ion affinity of the *CD–EF* domain (Agah *et al.*, 2003).

EF-hand proteins have been classified into two subclasses according to their function and affinity for ions (da Silva & Reinach, 1991). The first class contains proteins that have very high affinity for calcium and do not interact with other proteins in the cell. They are believed to act as calcium buffers (or containers) and their role is crucial in maintaining the proper low calcium concentration in the cytosol. The other subclass is calcium sensors, which have lower affinity for calcium and interact with other proteins upon calcium binding. They have several functions in the cell as regulators of target proteins (CaM, TnC), calcium-dependent enzymes (calpains) and proteins associated with the cytoskeleton (spectrin). Upon calcium binding, calcium-sensor proteins show important conformational changes: changes in interhelical angles and the exposure of hydrophobic patches. Calcium-buffer proteins such as calbindin D9K and parvalbumin have limited conformational changes upon calcium binding: there is no appreciable change in interhelical angles (only a few degrees) and a compact structure with no hydrophobic exposed patches (Ikura, 1996; Yap *et al.*, 1999). It is striking that limited conformational changes also apply to other domains that are not directly involved in ion binding. The PV salt bridge is a natural solution to limit the conformational flexibility of the *AB* loop and probably optimizes *AB* to *CD–EF* packing. The fluidity of hydrophobic cores in proteins plays the role of a lubricant in favouring the conformational rearrangements needed for the protein to function. Allosteric phenomena are among the most intriguing aspects of protein function and parvalbumin, with its functional EF-hand domain stacked on an autonomous structural element, may offer a useful model system for examining how remote determinants control ligand-binding events.

Thanks to Léonard Wong for protein preparation and crystallization experiments.

References

Agah, S., Larson, J. D. & Henzl, M. T. (2003). *Biochemistry*, **42**, 10886–10895.

Alattia, T., Padilla, A. & Cavé, A. (1996). *Eur. J. Biochem.* **237**, 561–574.

Baldellon, C., Alattia, J. R., Strub, M.-P., Pauls, T., Berchtold, M. W., Cavé, A. & Padilla, A. (1998). *Biochemistry*, **37**, 9964–9975.

Baldellon, C., Padilla, A. & Cavé, A. (1992). *Biochimie*, **74**, 837–844.

Bottoms, C. A., Schuermann, J. P., Agah, S., Henzl, M. T. & Tanner, J. J. (2004). *Protein Sci.* **13**, 1724–1734.

Brünger, A. T. (1993). *Acta Cryst.* D**49**, 24–36.

Cates, M. S., Berry, M. B., Ho, E. L., Li, Q., Potter, J. D. & Phillips, G. N. Jr (1999). *Structure*, **7**, 1269–1278.

Collaborative Computational Project, Number 4 (1994). *Acta Cryst.* D**50**, 760–763.

Cox, J. A., Milos, M. & MacManus, J. P. (1990). *J. Biol. Chem.* **265**, 6633–6637.

da Silva, A. C. & Reinach, F. C. (1991). *Trends Biochem. Sci.* **16**, 53–57.

Dong, F., Vijayakumar, M. & Zhou, H. X. (2003). *Biophys. J.* **85**, 49–60.

Drake, S. K. & Falke, J. J. (1996). *Biochemistry*, **35**, 1753–1760.

Drake, S. K., Zimmer, M. A., Miller, C. L. & Falke, J. J. (1997). *Biochemistry*, **36**, 9917–9926.

Emsley, P. & Cowtan, K. (2004). *Acta Cryst.* D**60**, 2126–2132.

Gillen, M. F., Banville, D., Rutledge, R. G., Narang, S., Seligy, V. L., Whitfield, J. F. & MacManus, J. P. (1987). *J. Biol. Chem.* **262**, 5308–5312.

Go, N., Noguti, T. & Nishikawa, T. (1983). *Proc. Natl Acad. Sci. USA*, **80**, 3696–3700.

Golden, L. F., Corson, D. C., Sykes, B. D., Banville, D. & MacManus, J. P. (1989). *J. Biol. Chem.* **264**, 20314–20319.

Goodman, M. & Pechere, J. F. (1977). *J. Mol. Med.* **9**, 131–158.

Gosselin-Rey, C., Bernard, N. & Gerday, C. (1973). *Biochim. Biophys. Acta*, **303**, 90–104.

Grove, A. (2003). *Biochemistry*, **42**, 8739–8747.

Hapak, R. C., Lammers, P. J., Palmisano, W. A., Birnbaum, E. R. & Henzl, M. T. (1989). *J. Biol. Chem.* **264**, 18751–18760.

Heizmann, C. W. (1984). *Experientia*, **40**, 910–921.

Henzl, M. T., Agah, S. & Larson, J. D. (2003). *Biochemistry*, **42**, 3594–3607.

Henzl, M. T., Agah, S. & Larson, J. D. (2004). *Biochemistry*, **43**, 10906–10917.

Henzl, M. T. & Graham, J. S. (1999). *FEBS Lett.* **442**, 241–245.

Henzl, M. T., Larson, J. D. & Agah, S. (2000). *Biochemistry*, **39**, 5859–5867.

Henzl, M. T., Larson, J. D. & Agah, S. (2003). *Anal. Biochem.* **319**, 216–233.

Henzl, M. T., Larson, J. D. & Agah, S. (2004). *Biochemistry*, **43**, 2747–2763.

Henzl, M. T. & Tanner, J. J. (2008). *Protein Sci.* **17**, 431–438.

Hubbard, S. J. & Thornton, J. M. (1993). *NACCESS Computer Program*, v.2.1.1. Department of Biochemistry and Molecular Biology, University College London, England.

Ikura, M. (1996). *Trends Biochem. Sci.* **21**, 14–17.

Kauffman, J. F., Hapak, R. C. & Henzl, M. T. (1995). *Biochemistry*, **34**, 991–1000.

Kissinger, C. R., Gehlhaar, D. K. & Fogel, D. B. (1999). *Acta Cryst.* D**55**, 484–491.
Kreiner, L. & Lee, A. (2006). *J. Biol. Chem.* **281**, 4691–4698.
Kretsinger, J. K. & Schneider, J. P. (2003). *J. Am. Chem. Soc.* **125**, 7907–7913.
Kretsinger, R. H. & Nockolds, C. E. (1973). *J. Biol. Chem.* **248**, 3313–3326.
Kumar, S. & Nussinov, R. (1999). *J. Mol. Biol.* **293**, 1241–1255.
Laskowski, R. A., Moss, D. S. & Thornton, J. M. (1993). *J. Mol. Biol.* **231**, 1049–1067.
Levitt, M., Sander, C. & Stern, P. S. (1985). *J. Mol. Biol.* **181**, 423–447.
Marqusee, S. & Sauer, R. T. (1994). *Protein Sci.* **3**, 2217–2225.
Marti, D. N. & Bosshard, H. R. (2003). *J. Mol. Biol.* **330**, 621–637.
McPhalen, C. A., Sielecki, A. R., Santarsiero, B. D. & James, M. N. (1994). *J. Mol. Biol.* **235**, 718–732.
McPhalen, C. A., Strynadka, N. C. & James, M. N. (1991). *Adv. Protein Chem.* **42**, 77–144.
Murphy, K. P. & Freire, E. (1992). *Adv. Protein Chem.* **43**, 313–361.
Nakayama, S., Moncrief, N. D. & Kretsinger, R. H. (1992). *J. Mol. Evol.* **34**, 416–448.
Palmisano, W. A., Trevino, C. L. & Henzl, M. T. (1990). *J. Biol. Chem.* **265**, 14450–14456.
Permyakov, E. A., Medvedkin, V. N., Mitin, Y. V. & Kretsinger, R. H. (1991). *Biochim. Biophys. Acta*, **1076**, 67–70.
Racay, P., Gregory, P. & Schwaller, B. (2006). *FEBS J.* **273**, 96–108.
Reynolds, G. P., Abdul-Monim, Z., Neill, J. C. & Zhang, Z. J. (2004). *Neurotox. Res.* **6**, 57–61.
Sakaguchi, N., Henzl, M. T., Thalmann, I., Thalmann, R. & Schulte, B. A. (1998). *J. Histochem. Cytochem.* **46**, 29–40.
Sarakatsannis, J. N. & Duan, Y. (2005). *Proteins*, **60**, 732–739.
Suhre, K. & Sanejouand, Y.-H. (2004*a*). *Acta Cryst.* D**60**, 796–799.
Suhre, K. & Sanejouand, Y.-H. (2004*b*). *Nucleic Acids Res.* **32**, W610–W614.
Szatkowski, M. L., Westfall, M. V., Gomez, C. A., Wahr, P. A., Michele, D. E., DelloRusso, C., Turner, I. I., Hong, K. E., Albayya, F. P. & Metzger, J. M. (2001). *J. Clin. Invest.* **107**, 191–198.
Thepaut, M., Strub, M.-P., Cavé, A., Banères, J. L., Berchtold, M. W., Dumas, C. & Padilla, A. (2001). *Proteins*, **45**, 117–128.
Wahr, P. A., Michele, D. E. & Metzger, J. M. (1999). *Proc. Natl Acad. Sci. USA*, **96**, 11982–11985.
Wnuk, W., Cox, J. A. & Stein, E. A. (1982). *Calcium and Cell Function*, edited by W. Y. Cheung, pp. 243–278. New York: Academic Press.
Wouterlood, F. G., Vinkenoog, M. & van den Oever, M. (2002). *Network*, **13**, 327–342.
Wu, Z., Li, X., de Leeuw, E., Ericksen, B. & Lu, W. (2005). *J. Biol. Chem.* **280**, 43039–43047.
Wüthrich, K. (1986). *NMR of Proteins and Nucleic Acids.* New York: John Wiley & Sons.
Xie, D. & Freire, E. (1994). *J. Mol. Biol.* **242**, 62–80.
Yano, J. K. & Poulos, T. L. (2003). *Curr. Opin. Biotechnol.* **14**, 360–365.
Yap, K. L., Ames, J. B., Swindells, M. B. & Ikura, M. (1999). *Proteins*, **37**, 499–507.
Zhou, J. & Xu, Z. (2003). *Nature Struct. Biol.* **10**, 942–947.